Optimised oscillating gradient diffusion MRI for the estimation of axon radius in an ex-vivo rat brain

Bernard Siow[1,2], Andrada Ianus[1], Ivana Drobnjak[1], Mark F Lythgoe[2,3], and Daniel C Alexander[1]

[1]Centre for Medical Image Computing, UCL, London, United Kingdom, [2]Centre for Advanced Biomedical Imaging, UCL, London, United Kingdom, [3]Institute of Child Health, UCL, London, United Kingdom

Introduction: We adapt the ActiveAx orientationally invariant axon radius index technique [1,2] for oscillating gradient spin-echo (OGSE) diffusion MRI. Reliable estimates of small axon radii (<5 µm) require high gradient amplitudes and short diffusion times, which limits the suitability of pulsed gradient spin-echo (PGSE) sequences for microstructure estimates in a clinical setting. OGSE sequences have shorter diffusion times and thus can probe shorter length scales [3-8]. A recent in silico study [8] suggests that the optimal gradient waveform for pore-size estimation, particularly for small radii, consists of oscillating trapezoids; [9] provides empirical support. In this study, we adapt the algorithm in [1] to optimize three separate protocols for axon radius index mapping with ActiveAx. The protocols are constructed from different types of OGSE sequences: sine normal (SN), cosine reversed (CR), and square wave(SW), as illustrated in Figure 1.We implemented these protocols on a 9.4T pre-clinical system and imaged an ex-vivo rat brain. We subsequently performed microstructure parameter fits for voxels in the corpus callosum. Parameter estimates were consistent across all OGSE protocols, producing highest radius index in the midbody. In addition, we found that the SWOGSE protocol consistently produced the narrowest posterior distributions on the fitted parameters, supporting the expected increase in sensitivity to the microstructural parameters.

Methods: **Optimisation**: The optimization framework was as described in [1,2,8]. The tissue model consisted of impermeable parallel cylinders with impermeable walls and an extra-axonal compartment, as described in [1,8]. The pulse sequences used were as in Figure 1 with a single spin echo readout. Here, we optimise the length, duration and frequency of the waveforms for a fixed gradient magnitude of 200 mTm^{-1}. The protocols were optimised for sensitivity to fibre radii of 0.5, 1, 2.5 & 5µm. The number of measurements per protocol was 6 in 60 directions (360 scans per protocol) plus 12 unweighted scans. **MRI**: The OGSE protocols were implemented on a 9.4T Agilent Technologies, Inc. pre-clinical system equipped with gradient capable of $1Tm^{-1}$ with a rise time of 200µs. A 26mm diameter Rapid Biomedical, GmBH r.f. coil was used. Imaging parameters are as follows: TR = 1.8s, TE = 65ms, 11 x 0.5mm slices, 5 dummy scans, 64x64 matrix, 20x20mm FoV. **Sample:** A Sprague Dawley rat brain was perfuse fixed using 4% paraformaldehyde (PFA) and stored in 4% PFA for 2 weeks. The sample was then suspended in 1% agarose in phosphate buffer solution. The sample temperature was maintained at 13.0±0.5°C during the scans. **Fitting:** A three stage fitting procedure detailed in [2] was used. Briefly this consisted of a grid search, gradient descent, and Markov Chain Monte Carlo (MCMC) procedures. An ex-vivo white matter tissue model described in [2] (zeppelin-cylinder-dot in the taxonomy in [10]) was used. Briefly, parallel cylinders of single radius, an extra axonal compartment, an isotropic CSF compartment, and a stationary trapped water compartment, with no exchange between the compartments. For the grid search and gradient descent all model parameters were fitted except diffusivity of the CSF compartment and free diffusivity inside and outside the cylinders (set to 2 and 0.6 $x10^{-9}$ m^2s^{-1}, respectively). The MCMC fitting had a runlength of 200000 and a burn-in of 10000, and only volume fraction and radius were fitted.

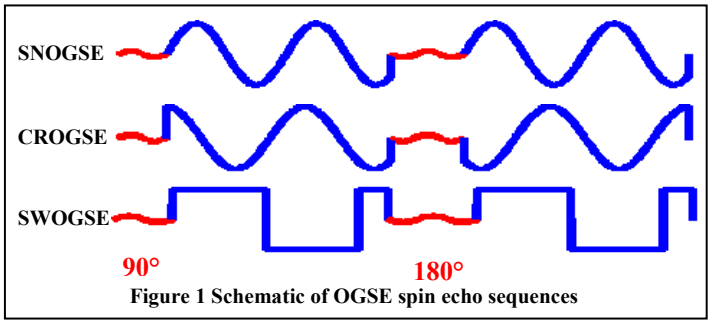

Figure 1 Schematic of OGSE spin echo sequences

Results and Discussion: **Posterior distributions:** Figure 2, shows the histograms of the posterior distribution on volume fraction and radius, taking every 200 samples of the MCMC run for signals averaged over a ROI covering the whole corpus callosum. We observe that the posterior distributions are consistent between protocols (overlapping distributions) and narrows from SNOGSE to CROGSE to SWOGSE, suggesting greater precision in the SWOGSE estimate. This trend was also observed for individual voxels (data not shown). CROGSE can produce rectangular waveforms by having a zero frequency, and thus diffusion weighting, whereas this is not possible with SNOGSE. We expect greater sensitivity from SWOGE because it packs more diffusion weighting into each period of the oscillation. Thus SNOGSE has ability to have greater attenuation at shorter length scales. **Parameter maps:** Figure 3 shows parameter maps of axon radius index and volume fraction over the mid-sagittal corpus callosum. We see that the axon radius index is consistently greatest in the midbody across all protocols. The trend is clearest with SWOGSE. The volume fraction decreases from anterior to posterior. These observations are consistent with previous studies [11,12].

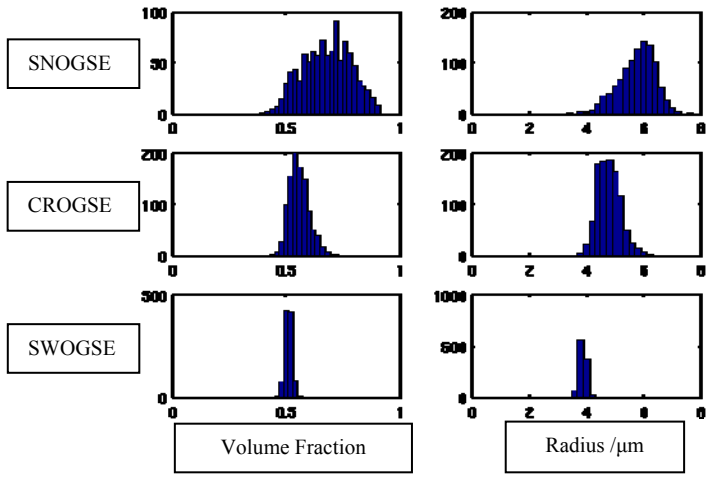

Figure 2 Histograms of posterior distributions on volume fraction and axon radius index

Conclusions: We have optimised SN-, CR-, & SW- OSGE protocols for ActiveAx allowing orientationally invariant axon radius index mapping, which we demonstrate in the corpus callosum of an ex-vivo rat. This is the first demonstration of OGSE to estimate axon radius. We find that the fitted parameters are consistent across all protocols, for example, finding that the axon radius is highest in the mid-body, which is consistent with previous literature using PGSE [2,12] . Future work will extend to in vivo and clinical scenarios: the total number of scans in each of the OGSE protocols (360+12) is achievable in those scenarios [2].

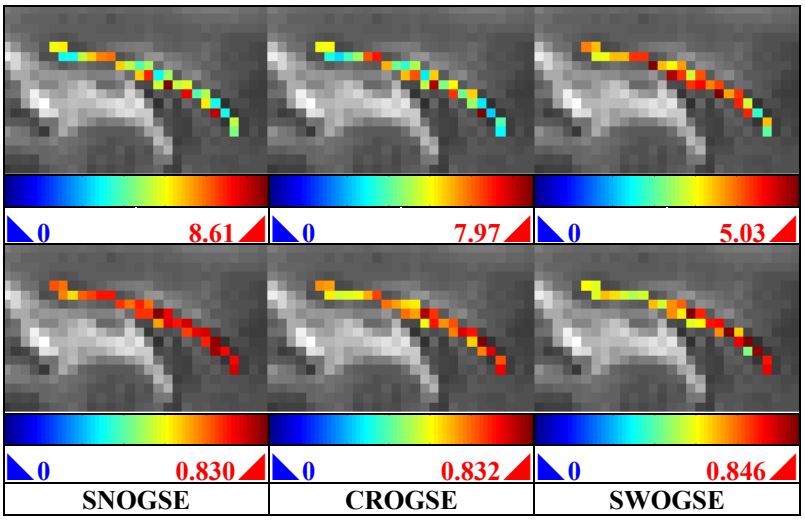

Figure 3 Axon radius index /µm (top row) and volume fraction (bottom row) maps

References [1] D Alexander, MRM 60 (2008) 439-448 [2] D Alexander, Neuroimage 52(4) (2011):1374-89 [3] J Xu, MRM 61 (2009) 828-833 [4] P Callaghan, Adv Magn Opt Reson 1996; 19:325–388 [5] E Parsons, Magn Reson Imaging 2003; 21: 279–285 [6] M Schachter, J Magn Reson 2000; 147: 232–237. [7] M Aggarwal, MRM 2011, in press [8] I Drobnjak, J Magn Res 206 (2010) 41-51 [9] B Siow, JMR 2011, in press [10] E Panagiotaki, Neuroimage 2011, in press [11] F Aboitiz, Brain Research 1992 598(1-2), 143-153 [12] D Barazany, Brain 132 (2009) 1210.